Annals of Physics 481 (2025) 170147

Contents lists available at ScienceDirect

Annals of Physics

journal homepage: www.elsevier.com/locate/aop

Warp bubble geometries with anisotropic fluids: A piecewise analytical approach

N. Bolívar [a,b,*], G. Abellán [a,b], I. Vasilev [b]

[a] Departamento de Física, Facultad de Ciencias, Universidad Central de Venezuela, Av. Los Ilustres, Caracas, 1041-A, Venezuela
[b] Astrum Drive Technologies, Dallas Pkwy Unit 120 B, Frisco, 75034, TX, USA

ARTICLE INFO

Keywords:
Warp drive
Warp bubble
Anisotropic fluids
General relativity
Energy conditions

ABSTRACT

We present a comprehensive analytical study of spherically symmetric warp bubble configurations in the framework of classical general relativity. We use a simplified ADM-type metric with a trivial lapse and a non-trivial radial shift function, which resembles a Painlevé–Gullstrand type metric. Employing this metric, our approach leads naturally to an anisotropic energy–momentum tensor characterized by an equation of state that emerges naturally from the equations. To reconcile the strict boundary conditions with the requirement of a localized matter distribution, we adopt a piecewise—defined model for the energy density. This construction allows us to confine possible violations of the dominant energy condition to finite and controlled shells, while ensuring that the weak and null energy conditions are globally satisfied. We illustrate our method with two representative examples: a one-shell exponential decay profile and a double-shell profile incorporating an additional power-law factor. Our results demonstrate that, by properly tuning the model parameters, it is possible to design warp bubble geometries that are not only mathematically consistent, but also physically more feasible, providing a promising stepping stone towards the development of realistic warp bubble models.

1. Introduction

Warp drive concepts, originally introduced by Alcubierre [1], have long captivated the theoretical physics community due to their promise of faster-than-light travel within the framework of general relativity. Despite their intriguing prospects, early models typically require exotic matter, often characterized by negative energy densities, to stabilize the warp-bubble geometry. Since then, various studies have aimed to explore modifications to the warp drive paradigm, either by altering the spacetime geometry [2–4] or by reconsidering the matter content under which energy constraints are satisfied [5–9].

The study of warp bubbles serves as key preliminary step in exploring warp drive geometries. In this article, we focus on the study of static warp bubble configurations, examining some geometries which can satisfy the classical energy conditions. Although typically associated with motion (often superluminal) in the standard warp drive literature, we use the term 'warp bubble' here in a broader sense, referring to any localized spacetime geometry characterized by an inner region with flat geometry and an outer curved region which is asymptotically flat. While the warp bubble presented in this study is indeed static and does not involve superluminal speeds, our goal is to clearly identify conditions under which the geometry and matter content can coexist without violating energy conditions. In this static setting, the piecewise—defined anisotropic model is particularly appealing as it maintains a positive energy density while satisfying essential energy conditions. This type of configuration can also serve as an appropriate initial

* Corresponding author at: Departamento de Física, Facultad de Ciencias, Universidad Central de Venezuela, Av. Los Ilustres, Caracas, 1041-A, Venezuela.
E-mail address: nelson.e.bolivar@ucv.ve (N. Bolívar).

https://doi.org/10.1016/j.aop.2025.170147
Received 18 April 2025; Accepted 1 July 2025
Available online 25 July 2025

condition for studying the evolution of matter shells, for instance, in scenarios involving the collapse or expansion of shells during the final stages of stellar evolution [10–14]. Moreover, by incorporating a notion of centroid motion into the current framework, one might eventually generalize the construction towards a moving warp bubble model—a version distinct from Alcubierre's original proposal since the energy density would remain positive.

By focusing on these localized spacetime structures, we can isolate the some key mechanisms underlying these spacetimes without resorting to overwhelmingly exotic matter distributions. Warp drive geometries generate great controversy due to their implications and consistent violation of classical energy conditions [15–27]. A detailed analysis of warp bubbles, particularly the interplay between the geometric framework and the anisotropic energy–momentum tensor, allows us to identify the necessary conditions for avoiding global energy condition violations, while confining any exotic features to localized regions. This understanding lays the groundwork for designing physically viable warp drive spacetimes, where a careful balance between necessary exotic matter and realistic energy conditions can potentially lead to models that are both mathematically consistent and physically plausible.

We choose a spherically symmetric configuration constructed using a simplified ADM-like metric with a trivial lapse function and a nontrivial radial shift $\beta(r)$ [28–30]. The emerging line element has certain similarities with the Painlevé–Gullstrand metric [31,32], which has been explored in previous studies given its high symmetry and ease of interpretation [33–39]. The resulting solutions demonstrate a carefully balanced interplay between geometry and matter, allowing for local solutions without invoking violations of the weak, strong, or null energy conditions. However, the price paid for this result is the introduction of non-differentiable features in the spacetime metric at certain hypersurfaces, where the left and right derivatives with respect to some coordinate of the metric fail to coincide. This non-differentiability may raise important questions about the physical viability of the solution.

We study a spherically symmetric bubble metric with a trivial lapse ($\alpha = 1$) and examine the resulting stress–energy and energy conditions. Our line element is

$$ds^2 = -dt^2 + \big(dr - \beta(r)\,dt\big)^2 + r^2\,d\theta^2 + r^2\sin^2\theta\,d\varphi^2\,. \tag{1}$$

We assume $|\beta(r)| < 1$ to avoid horizons. Schematically, our aim is:

- Derive the field equations in a local Minkowskian frame, showing $p_r = -\rho$ and $p_\perp$ expressed in terms of $\beta(r)$.
- Impose boundary conditions ($\rho(0) = 0$, $\beta(0) = 0$, $\rho(\infty) = 0$, $\beta(\infty) = 0$) and check if a single smooth $\rho(r)$ meets them without violating the classical energy requirements.
- Construct a piecewise model of $\rho(r)$ that resolves certain contradictions and examine which energy conditions are satisfied or violated in that piecewise solution.

In this paper, we outline the construction of warp bubble solutions, analyse the consequences of its non-differentiable regions, and discuss the implications for energy conditions and physical plausibility. We begin by describing a feasible solution for a warp bubble in spherical coordinates. Then we study the energy conditions for this solution. The effects of considering solutions that contain points where the spacetime is not derivable will now be studied. We then proceed to look at some illustrative examples. The first one considering a single discontinuity and a second example with two discontinuities. Finally we make a discussion of the results and venture some explanations and possible realizations of the obtained findings.

2. Einstein equations in spherical symmetry

We now want to explore the physical consequences of the proposed line element (1), for which we consider Einstein's equations

$$G_{\mu\nu} = 8\pi T_{\mu\nu}\,. \tag{2}$$

In order to be able to apply the warping procedure, we need a solution $\beta(r)$ for the static spacetime basis geometry. To find a solution we will switch to the local flat frame. For this, we use the following tetrad

$$(e^{\hat{0}})_\mu = (1,0,0,0)\,, \qquad (e^{\hat{1}})_\mu = (-\beta,1,0,0)\,, \tag{3}$$

$$(e^{\hat{2}})_\mu = (0,0,r,0)\,, \qquad (e^{\hat{3}})_\mu = (0,0,0,r\sin\theta)\,, \tag{4}$$

the index with hat is that on the local flat frame. Using this tetrad we write the Einstein equations in the local flat frame

$$\frac{\beta}{r^2}\Big(2r\,\beta' + \beta\Big) = 8\pi\rho\,, \tag{5}$$

$$-\frac{\beta}{r^2}\Big(2r\,\beta' + \beta\Big) = 8\pi p_r, \tag{6}$$

$$-\beta\,\beta'' - (\beta')^2 - 2\,\frac{\beta}{r}\,\beta' = 8\pi p_\perp\,. \tag{7}$$

From these equations, it can be seen that the matter sector corresponds to an anisotropic fluid with no heat flux or shear stresses. We can then describe the material sector as

$$T_{\hat{\alpha}\hat{\beta}} = \begin{pmatrix} \rho & 0 & 0 & 0 \\ 0 & p_r & 0 & 0 \\ 0 & 0 & p_\perp & 0 \\ 0 & 0 & 0 & p_\perp \end{pmatrix}. \tag{8}$$

Moreover, one can clearly notice an equation of state for matter with the form $p_r = -\rho$ arising naturally from Eqs. (5) and (6). This type of behaviour has already appeared in other warp bubble configurations [2].

3. Energy conditions

In order to achieve a physically feasible solution β, it is desirable to examine the restrictions imposed by the energy conditions on this function. For this purpose, we will used the usual general results definitions found for generic future-pointed observers in [4]. Note that we will consider all the expressions in the local flat frame.

3.1. Weak energy condition (WEC)

This requires that $T_{\hat{\alpha}\hat{\beta}}v^{\hat{\alpha}}v^{\hat{\beta}} \geq 0$ for a generic future-pointing timelike vector. We find that

$$\rho \geq 0\,, \qquad \rho + p_r \geq 0\,, \qquad \rho + p_\perp \geq 0\,. \tag{9}$$

So the weak energy condition is satisfied for any observer in the local frame if each of the above inequalities is satisfied. Since $\rho = -p_r$ it reduces to,

$$\rho \geq 0\,, \tag{10}$$

$$\rho + p_\perp \geq 0\,. \tag{11}$$

3.2. Strong energy condition (SEC)

The strong energy condition imposes a bound on the Ricci tensor $R_{\mu\nu}$ which yields an evaluation of the following expression $\left(T_{\hat{\alpha}\hat{\beta}} - \frac{1}{2}T\eta_{\hat{\alpha}\hat{\beta}}\right)v^{\hat{\alpha}}v^{\hat{\beta}} \geq 0$.

The following relations follow from this expression

$$\rho + p_r + 2p_\perp \geq 0\,, \qquad \rho + p_\perp \geq 0\,, \tag{12}$$

which again due the natural equation of state reduces to the relations,

$$p_\perp \geq 0\,, \tag{13}$$

$$\rho + p_\perp \geq 0\,. \tag{14}$$

3.3. Null energy condition (NEC)

The null energy condition $T_{\hat{\alpha}\hat{\beta}}k^{\hat{\alpha}}k^{\hat{\beta}} \geq 0$ is analogous to the weak condition but with the null vector $k^{\hat{\alpha}}$ replacing the time vector $v^{\hat{\alpha}}$. we obtain

$$\rho + p_r \geq 0\,, \qquad \rho + p_\perp \geq 0\,. \tag{15}$$

Using the equation of state, these equations reduces to

$$\rho + p_\perp \geq 0\,. \tag{16}$$

3.4. Dominant energy condition (DEC)

In this case, it is required that the expression $F^{\hat{\alpha}} = T^{\hat{\alpha}}_{\ \ \hat{\beta}}v^{\hat{\beta}}$ is a future-pointing causal vector. So that $F^{\hat{\alpha}}F_{\hat{\alpha}} \leq 0$ is fulfilled. That is

$$\rho^2 \geq 0\,, \qquad \rho^2 - p_r^2 \geq 0\,, \qquad \rho^2 - p_\perp^2 \geq 0\,, \tag{17}$$

and using $\rho = -p_r$, it simplifies to

$$\rho^2 \geq 0\,, \qquad \rho^2 - p_\perp^2 \geq 0\,. \tag{18}$$

In summary, the expressions that must be evaluated to study all the energy conditions are as follows

$$\rho \geq 0\,, \qquad p_\perp \geq 0\,, \qquad \rho + p_\perp \geq 0\,, \qquad \rho^2 - p_\perp^2 > 0\,. \tag{19}$$

We remark that the implication of a natural equation of state within the Einstein equations greatly facilitates the evaluation of the energy conditions.

4. Piecewise construction, boundary conditions and junction conditions

We now focus on additional constraints and boundary conditions, specifically ensuring that the energy density $\rho(r)$ and transverse pressure $p_\perp(r)$ satisfy physically reasonable boundary conditions. Since we are interested in the behaviour of the solutions within the different regions using the same metric ansatz, it is not necessary to use all the complexities of Israel's [40] or Lanczos' formalism [41]. Because of this we will use a straightforward approach to consider the different regions in order to reconstruct the whole spacetime. A complete treatment implies using Israel's formalism or a distributional formulation [42–47].

4.1. Constraints from Einstein's equations

The advantage of working with line element (1) using spherical symmetry is that Einstein's equations can formally be solved for the metric form function $\beta(r)$ and the transverse pressure $p_\perp(r)$ in terms of the energy density $\rho(r)$. From Eq. (5) we can integrate and find an expression for the beta function as follow

$$\beta^2 + 2r\beta\beta' = \frac{d}{dr}(r\beta^2) = 8\pi r^2\rho \quad \longrightarrow \quad \beta = \pm\sqrt{\frac{C}{r} + \frac{8\pi}{r}\int r^2\rho\, dr} \tag{20}$$

with C is an integration constant evaluated at some known point $r = r_0$. To get an expression for the tangential pressure we note that

$$\frac{d}{dr}(r^2\rho) = \frac{1}{8\pi}\frac{d}{dr}(\beta^2 + 2r\beta\beta') = \frac{2r}{8\pi}\left(\frac{2}{r}\beta\beta' + \beta'^2 + \beta\beta'\right). \tag{21}$$

Using Eq. (7) we can find a relation between the tangential pressure $p_\perp(r)$ and the energy density $\rho(r)$

$$p_\perp(r) = -\frac{1}{2r}\frac{d}{dr}\left[r^2\rho(r)\right], \tag{22}$$

The problem is thus reduced to providing the energy density. From Eq. (22), the condition $p_\perp(r) \geq 0$ implies that $r^2\rho(r)$ must be decreasing with r. In other words, $\rho(r)$ must drop faster than $1/r^2$. Note that any region in which $r^2\rho(r)$ increases unavoidably induces a sign change in $p_\perp(r)$.

To study how $\rho(r)$ changes, substitute Eq. (22) into condition $\rho + p_\perp \geq 0$. This leads to the requirement

$$\frac{d\rho(r)}{dr} \leq 0, \tag{23}$$

meaning energy density $\rho(r)$ is forced to be a nonincreasing function. If $\rho(r)$ decreases monotonically while remaining positive for $r \geq 0$, it does not meet the usual expectations for localized energy distributions in warp bubbles. This is because such a profile prevents the matter from forming a well-defined localized structure and instead imposes a strict radial monotonicity, which may not be physically realistic for this kind of system.

4.2. Thin shell analysis

To reconcile these constraints, we exploit a piecewise definition of $\rho(r)$ and $\beta(r)$. Next we will illustrate the procedure we are going to apply. Consider an energy density defined by

$$\rho(r) = \begin{cases} \rho_-(r), & 0 \leq r < r_0, \\ \rho_+(r), & r \geq r_0. \end{cases} \tag{24}$$

With this energy density, we find the metric shift function for each region, which gives us β_- and β_+. These solutions are written for the whole spacetime in the form

$$\beta(r) = \beta_-(r)\Theta(r_0 - r) + \beta_+(r)\Theta(r - r_0)\,, \tag{25}$$

where $\Theta(x)$ is the Heaviside step function. By convention we assume $\Theta(0) = 1/2$. Using the integration constant C appearing in (20), it is always possible to have a continuous spacetime, that is $\beta_-(r_0) = \beta_+(r_0)$. However, it is still possible to have jumps in first derivatives, so that $\beta'_-(r_0) \neq \beta'_+(r_0)$. Then, considering that the shift function β is continuous in $r = r_0$, we find the following expressions

$$\beta'(r) = \beta'_-(r)\Theta(r_0 - r) + \beta'_+(r)\Theta(r - r_0)\,, \tag{26}$$

$$\beta''(r) = \beta''_-(r)\Theta(r_0 - r) + \beta''_+(r)\Theta(r - r_0) + \left[\beta'_+(r) - \beta'_-(r)\right]\delta(r - r_0)\,. \tag{27}$$

We note that only Dirac delta-type terms appear in the second derivative. Therefore, both the energy density and the radial pressure will be continuous regular functions. In the case of tangential pressure, each case will have to be analysed in order to determine the regularity of the solution found.

By examining (7), we can see that the occurrence of thin shells of matter will be given by the term

$$\beta\beta'' = \beta_-\beta''_-\Theta_- + \beta_+\beta''_+\Theta_+ + \frac{1}{2}\left(\beta_- + \beta_+\right)\left(\beta'_+ - \beta'_-\right)\delta(r - r_0)\,, \tag{28}$$

where $\Theta_- = \Theta(r_0 - r)$, $\Theta_+ = \Theta(r - r_0)$. Since in $r = r_0$ the relation $\beta_-(r_0) = \beta_+(r_0) = 0$ is satisfied, we can see that the term proportional to the Dirac delta vanishes and thus the solution has no thin shells.

The piecewise approach solves the problematic behaviour when increasing from $r = 0$ in a standard way that is well grounded in the literature. By setting $\rho(r < r_0) = 0$, we circumvent the issue of forcing $\rho(0)$ and $\beta(0)$ to remain finite (and, in our case, zero). At the same time, we are then free to tune the matter shell at $r \geq r_0$ to fulfil the boundary conditions $\beta(r \to \infty) = 0$. Although such simplifications may omit some subtle effects near r_0, they greatly reduce technical complications and allow us to focus on the main physical objectives of the warp-bubble analysis. We stress, however, that any truly rigorous configuration should verify, via the Israel junction conditions, that no unaccounted-for surface energy distributions arise when transitioning from a vacuum (inner region) to a nonvacuum (outer region) solution. In this work we are only interested in the behaviour of solutions outside the singularities.

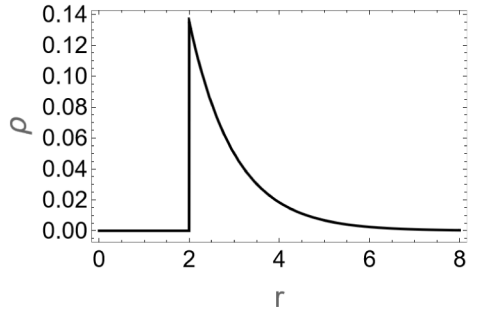

(a) Energy density ρ profile. Exponential decay.

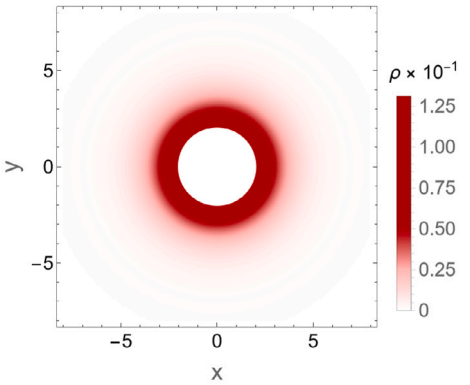

(b) Energy density ρ 2D map. Emphasize the radial symmetry.

Fig. 1. Energy density for single shell bubble with $a = 1$ and $b = 1$.

5. Illustrative examples

Let us examine some concrete realizations of the formal solution found above. For this purpose, we must provide a concrete form of the energy density.

5.1. Piecewise-exponential (single shell profile)

A simple choice for the energy density functional form that satisfies the aforementioned criteria is

$$\rho(r) = \begin{cases} 0, & 0 \le r < \frac{2}{b}\,, \\ a\,e^{-br}, & r \ge \frac{2}{b}\,, \end{cases} \tag{29}$$

where $a > 0$ and $b > 0$. The parameter a controls the amplitude (or overall scale) of the energy density in the outer region, whereas b controls how quickly the energy density ρ decays as r increases. Large b makes the energy distribution narrower and more sharply peaked just beyond $r = \frac{2}{b}$, while smaller b spreads the bubble over a thicker region.

Once the realization for the energy density is given, we proceed to calculate the rest of the quantities in the model. For $r < 2/b$, $\beta(r) = 0$, and the spacetime is flat (vacuum solution $\rho = p_r = p_\perp = 0$). For $r \ge 2/b$, the metric function $\beta(r)$ is determined (20). Specifically

$$\beta(r) = \sqrt{\frac{8\pi a}{b^3 r}\left[10e^{-2} - e^{-br}(b^2r^2 + 2br + 2)\right]}\,, \tag{30}$$

$$p_\perp = \frac{1}{2}abe^{-br}\left(r - \frac{2}{b}\right). \tag{31}$$

Here we have chosen the constant of integration in such a way that the continuity of β at point $r = 2/b$ is guaranteed. Note that one can show that, by suitable choices of parameters a and b, we can keep $|\beta(r)| < 1$, ensuring no horizons.

In order to check whether the solution contains thin shells, we examine the expressions (5)–(7) together with the relations (25)–(27). Since we only need β and β' to obtain ρ and p_r, we see that none of these expressions contain terms proportional to the Dirac delta function. Finally, since $\beta(2/b) = 0$, the term proportional to the Dirac delta in (28) vanishes and therefore the tangential pressure $p_\perp$ does not contain singularities either. Thus we conclude that the entire material sector is regular for the obtained solution.

Figs. 1–3 show the quantities $\rho(r)$, $\beta(r)$ and $p_\perp(r)$ respectively. A null inner region is clearly visible. Then, at the critical point, there is the discontinuity. We can notice that for $\rho(r)$ and $p_\perp(r)$, the discontinuity is a jump discontinuity. However, the discontinuity is in the first derivative for $\beta(r)$. After this critical point onwards, the system has the configuration given by the non-trivial part of the solutions.

5.2. Energy condition for the piecewise-exponential profile

We now proceed to examine the energy conditions for this system in each of the regions defined by the solution found.

WEC. We recall that condition $\rho + p_r \ge 0$ is trivially satisfied given the natural equation of state of this system. Therefore it demands $\rho \ge 0$ and $\rho + p_\perp \ge 0$, which is satisfied in the outer region, and trivially zero inside. Hence the WEC is obeyed throughout.

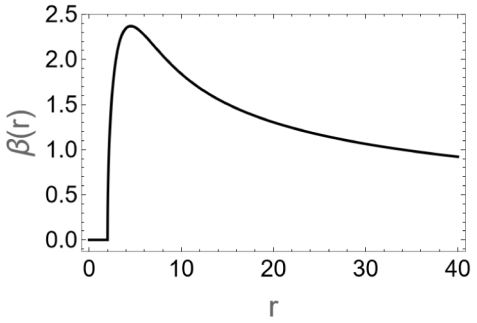

(a) Shift function β profile. In $0 < r < 2/b$, $\beta = 0$. At large r, $\beta \to 0$.

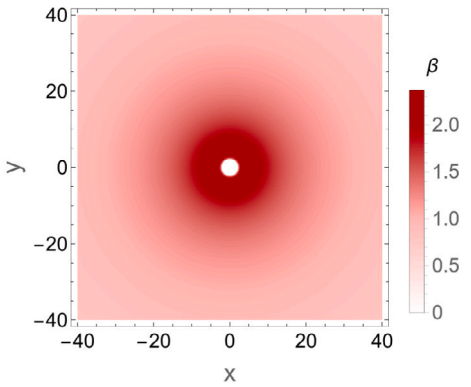

(b) Shift function β 2D map. Emphasize the radial symmetry.

Fig. 2. Form function $\beta(r)$ for single shell bubble with $a = 1$ and $b = 1$.

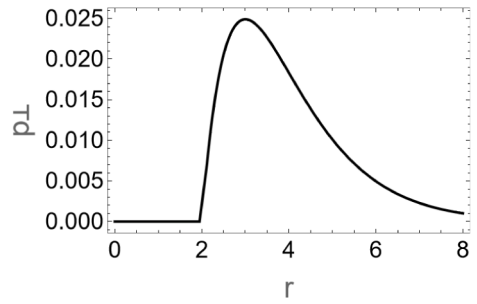

(a) Tangential pressure $p_\perp$ profile. Zero inner region and the nontrivial region for $r \geq 2/b$.

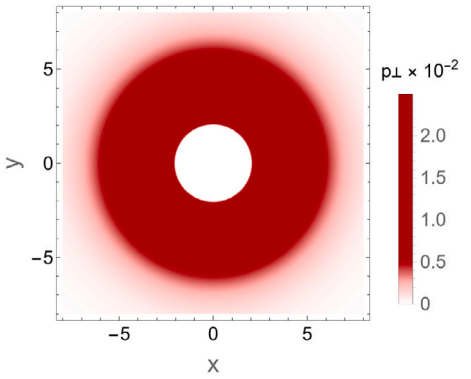

(b) Tangential pressure $p_\perp$ 2D map. Emphasize the radial symmetry.

Fig. 3. Tangential pressure for single shell bubble with $a = 1$ and $b = 1$.

SEC. This requires $p_\perp > 0$. We can compute $p_\perp$ from

$$p_\perp(r) = -\frac{(r^2\rho(r))'}{2r}. \tag{32}$$

In the inner region it is automatically satisfied. In the outer, if $r^2\rho(r)$ is decreasing on any interval, then $p_\perp > 0$ there, satisfying the SEC. Indeed, for the exponential tail, we typically find positive $p_\perp$, so the SEC is sustained in that region. It is worth to emphasize that for any choices of a and b, if $r^2\rho(r)$ increases in some interval, it will lead to negative $p_\perp$. Hence the SEC can be violated. Typically, $p_\perp$ becomes negative around the in-out-transition, indicating partial exoticity.

NEC. Since $\rho + p_r = \rho - \rho = 0$, the NEC is always saturated at 0.

DEC. The DEC imposes one additional constraint, $\rho^2 - p_\perp^2 \geq 0$,

We analyse two separate regions:

1. Region $r < \frac{2}{b}$*:.* The DEC is trivially satisfied for $r < \frac{2}{b}$.

2. Region $r \geq \frac{2}{b}$*:.* We have to check the relation $\rho^2 - p_\perp^2 \geq 0$. For this we use the expressions (29) and (31). After some algebra we find,

$$\rho^2(r) - p_\perp^2(r) = a^2\, e^{-2\,b\,r}\left[1 - \frac{1}{4}\left(2 - b\,r\right)^2\right] \geq 0\,. \tag{33}$$

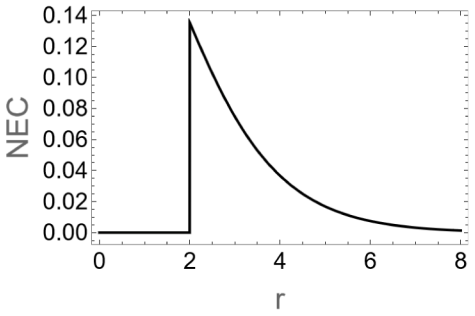

(a) Null Energy Condition.

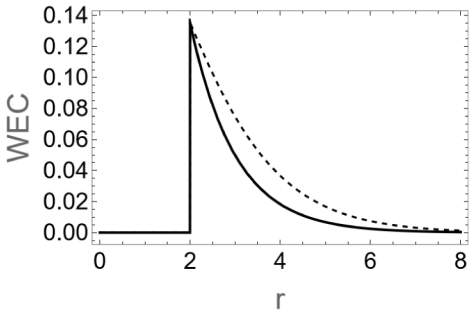

(b) Weak energy condition. The continuous lines corresponds to ρ and the dashed line is $\rho + p_{\perp}$.

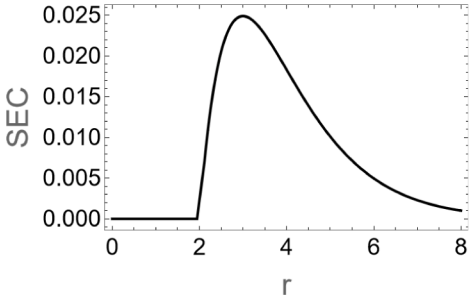

(c) Strong Energy Condition.

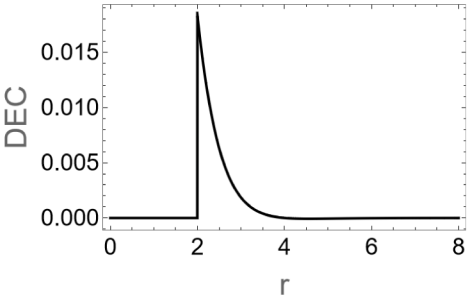

(d) Dominant Energy Condition.

Fig. 4. Energy conditions for single shell bubble with $a = 1$ and $b = 1$.

Since we know that $a^2 > 0$ and $e^{-2br} > 0$, we see that the following must be true

$$1 - \frac{(2 - br)^2}{4} \geq 0 \qquad \Longrightarrow \qquad 0 \leq r \leq \frac{4}{b}\,. \tag{34}$$

Therefore, the DEC is also strictly satisfied within the annular region $\frac{2}{b} \leq r \leq \frac{4}{b}$, and fails for $r > \frac{4}{b}$. Note that the dominant factor when it fails is e^{-2br}, so it vanishes fast as r increases.

Hence, this particular piecewise-exponential profile satisfies the WEC, the SEC, and saturates the NEC. The DEC is strictly satisfied only in the localized shell. The degree of violation/satisfaction depends on a and b. Larger a or smaller b can increase negative DEC regions. Fig. 4 illustrates the behaviour of the energy conditions. There it is verified that they are satisfied for this one-layer model except for the DEC.

To solve this DEC violation we can consider a second shell in $r = 4/b$. By doing this, for the region $r > 4/b$ the energy density becomes zero and therefore also the tangential pressure, so that the energy condition is satisfied in the whole domain. To clearly illustrate this procedure, we will work in detail the following example.

5.3. Exponential/power law decay piece-wise (double shell profile)

The previous results regarding the DEC suggest that a construction where three regions are defined could amend the energy conditions satisfaction issues. Guided by this, we can propose a layer-type of energy density structure. Specifically, we choose

$$\rho(r) = \begin{cases} 0, & 0 \leq r < R, \\ \dfrac{A\,\exp\left[-b\,(r - R)\right]}{r^2}, & R \leq r \leq \frac{2}{b}, \\ 0, & r > \frac{2}{b}, \end{cases} \tag{35}$$

with $A > 0$, $b > 0$, and $R > 0$ chosen such that $R < \frac{2}{b}$.

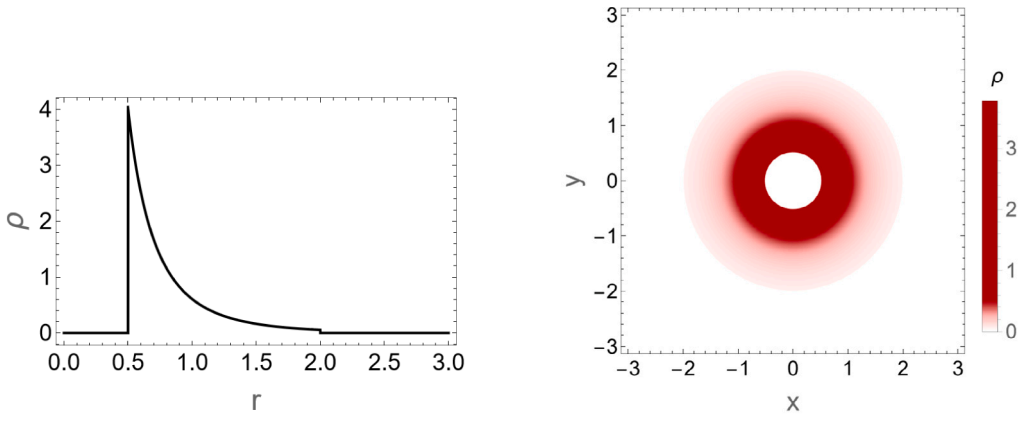

(a) Energy density ρ profile. Exponential decay with amplitude a and rate b.

(b) Energy density ρ 2D map. Emphasize the radial symmetry.

Fig. 5. Energy density for double shell bubble with $a = 1$, $b = 1$ and $R = b/2$.

Consider the realization for the energy density (35), the general expressions for the metric function (20) and the tangential pressure (22). Performing the procedure for both critical points, we can find

$$\beta(r) = \begin{cases} 0, & \text{for } 0 \le r < R, \\ \sqrt{\frac{8\pi}{r}\,\frac{A}{b}\left[1-\exp\left(-b(r-R)\right)\right]}, & \text{for } R \le r \le \frac{2}{b}, \\ \sqrt{\frac{8\pi}{r}\,\frac{A}{b}\left[1-\exp\left(-b\left(\frac{2}{b}-R\right)\right)\right]}, & \text{for } r > \frac{2}{b} \end{cases}$$

$$p_\perp(r) = \begin{cases} 0, & \text{for } 0 \le r < R, \\ \frac{Ab}{2r}\,\exp\left[-b\,(r-R)\right], & \text{for } R \le r \le \frac{2}{b}, \\ 0, & \text{for } r > \frac{2}{b} \end{cases} \tag{36}$$

It is worth noting that although $\rho(r)$ is zero for $r > 2/b$, the definite integral $\int_0^r \rho(r')\, r'^2\, \mathrm{d}r'$ accumulates a nonzero constant when r reaches $2/b$ and thereby one has a non-trivial vacuum solution for $r > 2/b$. This solution is asymptotically flat. This can be interpreted as a non-local effect of the energy density on the shape of spacetime.

To investigate whether the solution is regular or has thin shells of matter, we must examine it at both critical points. First of all, when considering the behaviour in $r = R$, we see that the analysis is completely analogous to the previous example. And so we can say that the solution is regular at this point. However, the behaviour at $r = 2/b$ is different. Although ρ and p_r are regular and do not have thin shells, we can see that the tangential pressure has a singular behaviour. This is caused by the fact that, although β is continuous in $r = 2/b$, its value does not become zero $\beta(2/b) \neq 0$ and therefore the term proportional to the Dirac delta in (28) does not vanish. Therefore, this solution has a thin shell in the tangential pressure $p_\perp$ at the point $r = 2/b$.

We can find the expression for the tangential pressure $p_\perp$ in the region $r > 2/b$ using the Einstein equation (7) and the (25)–(28) relations. By doing the calculations we find that

$$\begin{aligned} p_\perp(r) &= -\frac{\beta(2/b)}{8\pi}\left[\beta'_+(2/b) - \beta'_-(2/b)\right]\delta(r-2/b) \\ &= \frac{bA}{4}e^{-b\left(\frac{2}{b}-R\right)}\delta(r-2/b)\,, \end{aligned} \tag{37}$$

with β_- the solution for $R \le r \le 2/b$ and β_+ the solution for $r > 2/b$. As is usual when these singular behaviours appear in the metric, these thin shells must be added to the material sector in such a way that the geometry and the corresponding matter become consistent.

Figs. 5–7 show the quantities $\rho(r)$, $\beta(r)$, $p_\perp(r)$ respectively, for the double shell solution. Again, an internal null region is observed. At the first critical point $r = R$, there is a discontinuity. We can notice that for $\rho(r)$ and $p_\perp(r)$, the discontinuity is a jump discontinuity. However, for $\beta(r)$, the discontinuity is in the first derivative. The same type of behaviour is observed at the second critical point $r = 2/b$. After this critical point onwards the system has the configuration given by the non-trivial part of the solutions found. It is important to note that in the outer region of both solutions the spacetime is still curved although the material content has already vanished.

5.4. Energy conditions for the exponential/power law decay (double shell profile)

We now proceed to examine the energy conditions for this solution which contains two critical points in its domain.

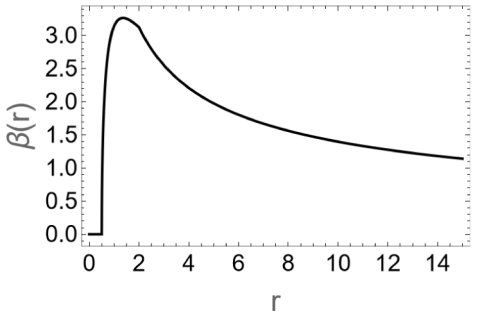

(a) Form function β profile. In $0 < r < 2/b$, $\beta = 0$. Then it grows and $\beta \to 0$ at large r.

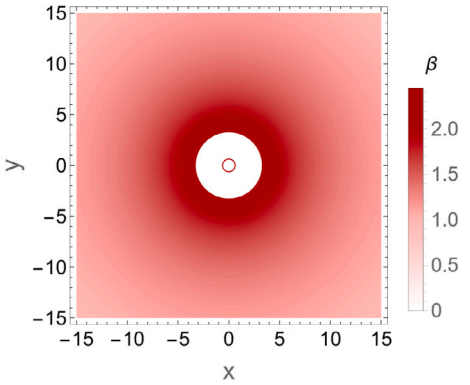

(b) Form function β 2D map. Emphasize the radial symmetry.

Fig. 6. Form function for double shell bubble with $a = 1$, $b = 1$ and $R = b/2$.

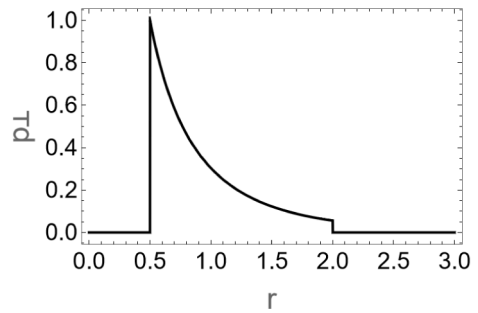

(a) Tangential pressure $p_\perp$ profile. Zero inner region and the nontrivial region for $r \geq 2/b$.

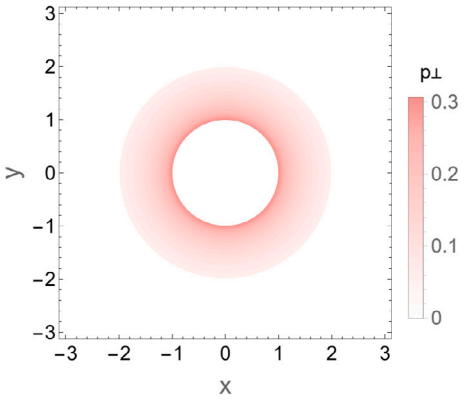

(b) Tangential pressure $p_\perp$ 2D map. Emphasize the radial symmetry.

Fig. 7. Tangential pressure for double shell bubble with $a = 1$, $b = 1$ and $R = b/2$.

Region I: $0 \leq r < R$. Since $\rho(r) = 0$ in the inner (vacuum) region, we have

$$r^2\,\rho(r) = 0 \quad \Rightarrow \quad \frac{d}{dr}\left[r^2\,\rho(r)\right] = 0\,, \tag{38}$$

so that from Eq. (22) it follows that $p_\perp(r) = 0$.

Thus, $\rho(r) = 0$ and $p_\perp(r) = 0$ imply that conditions (19) are trivially satisfied.

Region II: $R \leq r \leq \frac{2}{b}$. In this "outer-shell" region the energy density is nonzero:

$$\rho(r) = \frac{A\,\exp\left[-b\,(r-R)\right]}{r^2} > 0\,, \tag{39}$$

so that condition $\rho \geq 0$ holds. A brief calculation shows that

$$p_\perp(r) = -\frac{1}{2r}\left[-A\,b\,\exp\left[-b\,(r-R)\right]\right] = \frac{A\,b}{2r}\,\exp\left[-b\,(r-R)\right]\,. \tag{40}$$

Since $r > 0$ and all constants are positive, we have $p_\perp(r) > 0$. Furthermore, by direct addition,

$$\rho(r) + p_\perp(r) = A\,\exp[-b(r-R)]\left[\frac{1}{r^2} + \frac{b}{2r}\right] > 0\,. \tag{41}$$

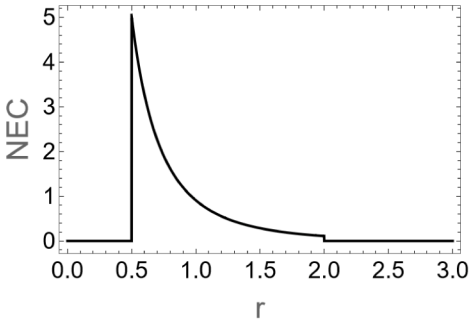

(a) Null Energy Condition.

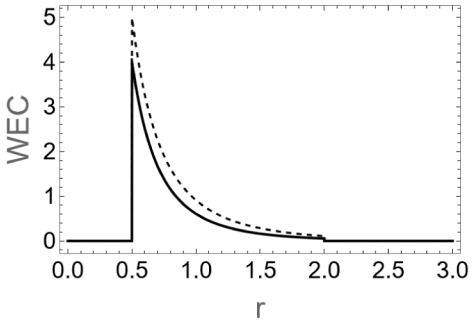

(b) Weak energy condition. The continuous lines corresponds to ρ and the dashed line is $\rho + p_\perp$.

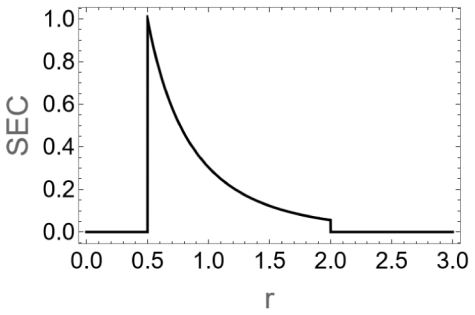

(c) Strong Energy Condition.

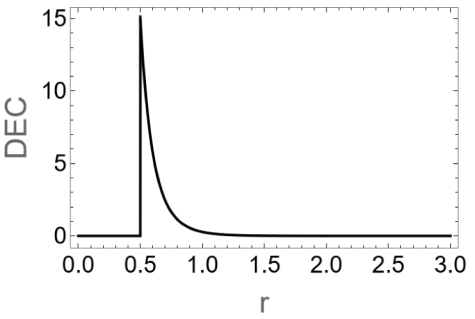

(d) Dominant Energy Condition.

Fig. 8. Energy conditions for double shell bubble with $a = 1$, $b = 1$ and $R = b/2$.

Finally, we obtain that

$$\rho(r)^2 - p_\perp(r)^2 = \frac{A^2 \exp[-2b(r-R)]}{r^4}\left[1 - \frac{b^2 r^2}{4}\right]. \tag{42}$$

Given that $r \leq \frac{2}{b}$ implies $b^2 r^2 \leq 4$, the bracket is nonnegative (and null only at the boundary $r = \frac{2}{b}$). Hence, $\rho(r)^2 - p_\perp(r)^2 > 0$ in this middle region.

We have been able to verify that all energy conditions in (19) are satisfied in the region where the active matter is located.

Region III: $r > \frac{2}{b}$. In this region the energy $\rho(r)$ density is reset to zero, so that tangential pressure $p_\perp(r)$ also vanishes. Therefore, all conditions in (19) hold trivially (see Fig. 8).

6. Discussion

We have seen how, by considering a piece-wise defined configuration of matter, it is possible to generate solutions for warp bubbles that satisfy the classical energy conditions. A remarkable aspect of this is that the geometry remains continuous, showing discontinuities only in the first derivative.

The piecewise solutions allow one to handle the problems that usually arise in the energy conditions by confining the matter to localized regions. Although some exoticity (local violations of the energy conditions) is introduced in the single shell model, this can be minimized by a convenient choice of solution parameters. The double shell model is very interesting, as it satisfies all energy conditions and in particular the weak energy condition (WEC), thus eliminating the need for exotic matter.

The proposed system is consistent with equation of state $p_r = -\rho$. It emerges naturally from Einstein's equations. Since in the proposed solutions the energy density is always positive, this implies negative radial pressures. Moreover, we note that in general $p_\perp$ is positive (at least in a large region of the domain for the single shell model) and $p_\perp \neq \rho$.

Solutions with negative radial pressure may be an indication of exoticity of the solution. For example, anisotropic dark energy can be modelled using the anisotropic fluid model by adding the equation of state $p_r = -\rho$ (for more details, see [48–51]).

In the particular piecewise-exponential solution (single shell), the parameters (a, b) allow one to tune the density amplitude and the radial scale of the bubble. Larger a or smaller b intensifies the total integrated energy density in the shell, potentially making the violation of the DEC pronounced. The single shell example shows a natural region where DEC is satisfied, that is $\frac{2}{b} \leq r \leq \frac{4}{b}$ of

active matter, and it fails for $r > \frac{4}{b}$. The functional dependence is dominated by $\sim e^{-br}$, which puts under some control the DEC violation and is always rapidly decaying. Moreover, a narrower or lower-amplitude bubble might reduce the magnitude of exotic pressures but at the cost of concentrating energy in a smaller region. As the tangential pressure depends on the derivative of the energy density, there is this interplay in the behaviour of the quantities.

Perhaps a more conventional interpretation, which does not require calling the appearance of exotic matter, would be to consider that the material content is composed of a charged anisotropic fluid. In this case also the condition $p_r = -\rho$ has to be fulfilled, but not necessarily $p_\perp = \rho$ (as is the case in our model). This possibility is interesting because it allows the material content to be interpreted in a way that reduces the degree of exoticity of the energy momentum tensor content (see the discussion in [52–56] for a deeper analysis). However, from a physical perspective, some exoticity remains. The bubble can therefore be considered to be "less exotic" than models of unconstrained exotic matter, since no negative ρ is required. This is important since models with positive energy densities (that meet the WEC) are more reliable candidates for representing physically viable models. In Section 4, we detailed how by imposing the continuity of $\beta(r)$ at the critical points, adjusting the integration constants, the delta-function contributions emerging from the discontinuities in the first derivatives are effectively cancelled. This precise matching guarantees that the energy density and radial pressures remain regular across the hypersurfaces—even when the derivative of the metric is discontinuous. However, for tangential pressure, a careful analysis of each case must be carried out in order to determine the presence of singular behaviours.

7. Final remarks

In this work, we have derived multiple analytical solutions for warp bubble geometries by relaxing conventional differentiability requirements, a methodological departure from prior approaches. These solutions reveal critical insights into the interplay between spacetime engineering and energy condition viability. Notably, while the static warp bubble configuration inherently satisfies all classical energy conditions.

We have derived and analysed several analytical solutions for a spherically symmetric warp bubble within the framework of classical general relativity. The derivation naturally yields an energy–momentum tensor characterized by an anisotropic fluid with a radial pressure $p_r = -\rho$ and tangential pressures $p_\perp$ that, in general, differ from ρ. This structure is crucial for sustaining the warp bubble geometry and illustrates the need for a type of matter distributions that may have some degree of exoticity although this is not necessarily the case as we have already discussed.

Our analysis shows that by including a discontinuity the proposed solutions can be arranged to satisfy the weak energy condition (WEC) and the zero energy condition (NEC) globally, while the strong energy condition (SEC) is satisfied in regions where the tangential pressure remains positive. Although the DEC can be violated in localized areas, this exoticity is confined and can be minimized by appropriate tuning of the model parameters. By relaxing the differentiability requirements in the ordinary sense in at least two points of the domain, we find that it is possible to fully satisfy the energy conditions.

The study provides some insights into how warp engine geometries could be sustained without relying entirely on negative energy densities. By carefully balancing the contributions of anisotropic fluids and potentially combining them with additional fields, such as electromagnetic sources, it is possible to design a configuration of matter that meets the necessary geometrical and physical requirements.

In summary, our analytical investigation highlights that piecewise-defined warp bubble solutions offer a promising route towards constructing more physically viable structures like warp drive models. While challenges remain—particularly regarding smoothness and the handling of localized energy condition violations—the insights gained here pave the way for future explorations into dynamical extensions and stability analyses that could further enhance the feasibility of this kind of spacetimes.

CRediT authorship contribution statement

N. Bolívar: Writing – review & editing, Writing – original draft, Supervision, Investigation, Formal analysis, Conceptualization. **G. Abellán:** Writing – review & editing, Writing – original draft, Investigation, Formal analysis. **I. Vasilev:** Formal analysis, Conceptualization.

Declaration of competing interest

The authors declare that they have no known competing financial interests or personal relationships that could have appeared to influence the work reported in this paper.

Data availability

No data was used for the research described in the article.

References

[1] M. Alcubierre, The Warp drive: Hyperfast travel within general relativity, Cl. Quant. Grav. 11 (1994) L73–L77, http://dx.doi.org/10.1088/0264-9381/11/5/001, arXiv:gr-qc/0009013.
[2] G. Abellan, N. Bolivar, I. Vasilev, Influence of anisotropic matter on the alcubierre metric and other related metrics: revisiting the problem of negative energy, Gen. Relativity Gravitation 55 (4) (2023) http://dx.doi.org/10.1007/s10714-023-03105-8.
[3] G. Abellan, N. Bolivar, I. Vasilev, Alcubierre warp drive in spherical coordinates with some matter configurations, Eur. Phys. J. C 83 (1) (2023) 7, http://dx.doi.org/10.1140/epjc/s10052-022-11091-5.
[4] G. Abellán, N. Bolívar, I. Vasilev, Spherical warp-based bubble with non-trivial lapse function and its consequences on matter content, Classical Quantum Gravity 41 (10) (2024) 105011, http://dx.doi.org/10.1088/1361-6382/ad3ed9.
[5] O.L. Santos-Pereira, E.M.C. Abreu, M.B. Ribeiro, Dust content solutions for the alcubierre warp drive spacetime, Eur. Phys. J. C 80 (8) (2020) 786, http://dx.doi.org/10.1140/epjc/s10052-020-8355-2, arXiv:2008.06560.
[6] O.L. Santos-Pereira, E.M.C. Abreu, M.B. Ribeiro, Perfect fluid warp drive solutions with the cosmological constant, Eur. Phys. J. Plus 136 (9) (2021) 902, http://dx.doi.org/10.1140/epjp/s13360-021-01899-7, arXiv:2108.10960.
[7] O.L. Santos-Pereira, E.M.C. Abreu, M.B. Ribeiro, Charged dust solutions for the warp drive spacetime, Gen. Relativity Gravitation 53 (2) (2021) 23, http://dx.doi.org/10.1007/s10714-021-02799-y, arXiv:2102.05119.
[8] O.L. Santos-Pereira, E.M.C. Abreu, M.B. Ribeiro, Warp drive dynamic solutions considering different fluid sources, in: 16th Marcel Grossmann Meeting on Recent Developments in Theoretical and Experimental General Relativity, Astrophysics and Relativistic Field Theories, 2021, arXiv:2111.01298.
[9] O.L. Santos-Pereira, E.M.C. Abreu, M.B. Ribeiro, Fluid dynamics in the warp drive spacetime geometry, Eur. Phys. J. C 81 (2) (2021) 133, http://dx.doi.org/10.1140/epjc/s10052-021-08921-3, arXiv:2101.11467.
[10] M. Castagnino, N. Umerez, On the dynamics of a thin spherically symmetric radiating shell, its classical model, and relativistic effects, Gen. Relativity Gravitation 15 (7) (1983) 625–634, http://dx.doi.org/10.1007/BF00759039.
[11] J.S. Hoye, I. Linnerud, K. Olaussen, R. Sollie, Evolution of Spherical Shells in General Relativity, Phys. Scr. 31 (1985) 97, http://dx.doi.org/10.1088/0031-8949/31/2/001.
[12] D. Nunez, H.P. De Oliveira, Dynamics of massive shell ejected in a supernova explosion, 1994, arXiv:astro-ph/9404055.
[13] J.P. Krisch, E.N. Glass, Thin Shell Dynamics and Equations of State, Phys. Rev. D 78 (2008) 044003, http://dx.doi.org/10.1103/PhysRevD.78.044003, arXiv:0808.0475.
[14] V. Cardoso, J.V. Rocha, Collapsing shells, critical phenomena and black hole formation, Phys. Rev. D 93 (8) (2016) 084034, http://dx.doi.org/10.1103/PhysRevD.93.084034, arXiv:1601.07552.
[15] K.D. Olum, Superluminal travel requires negative energies, Phys. Rev. Lett. 81 (1998) 3567–3570, http://dx.doi.org/10.1103/PhysRevLett.81.3567, arXiv:gr-qc/9805003.
[16] R.J. Low, Speed limits in general relativity, Cl. Quant. Grav. 16 (1999) 543–549, http://dx.doi.org/10.1088/0264-9381/16/2/016, arXiv:gr-qc/9812067.
[17] C. Barcelo, M. Visser, Scalar fields, energy conditions, and traversable wormholes, Cl. Quant. Grav. 17 (2000) 3843–3864, http://dx.doi.org/10.1088/0264-9381/17/18/318, arXiv:gr-qc/0003025.
[18] C. Barcelo, M. Visser, Twilight for the energy conditions? Internat. J. Modern Phys. D 11 (2002) 1553–1560, http://dx.doi.org/10.1142/S0218271802002888, arXiv:gr-qc/0205066.
[19] F. Lobo, P. Crawford, Weak energy condition violation and superluminal travel, in: L. Fernandez-Jambrina, L.M. Gonzalez-Romero (Eds.), Lect. Notes Phys. 617 (2003) 277–291, arXiv:gr-qc/0204038.
[20] F.S.N. Lobo, M. Visser, Fundamental limitations on 'warp drive' spacetimes, Cl. Quant. Grav. 21 (2004) 5871–5892, http://dx.doi.org/10.1088/0264-9381/21/24/011, arXiv:gr-qc/0406083.
[21] B. McMonigal, G.F. Lewis, P. O'Byrne, The Alcubierre Warp Drive: On the Matter of Matter, Phys. Rev. D 85 (2012) 064024, http://dx.doi.org/10.1103/PhysRevD.85.064024, arXiv:1202.5708.
[22] M. Alcubierre, F.S.N. Lobo, Wormholes, Warp Drives and Energy Conditions, vol. 189, Springer, 2017, http://dx.doi.org/10.1007/978-3-319-55182-1, arXiv:2103.05610.
[23] E.W. Lentz, Breaking the warp barrier: hyper-fast solitons in Einstein–Maxwell-plasma theory, Cl. Quant. Grav. 38 (7) (2021) 075015, http://dx.doi.org/10.1088/1361-6382/abe692, arXiv:2006.07125.
[24] J. Santiago, S. Schuster, M. Visser, Generic warp drives violate the null energy condition, Phys. Rev. D 105 (6) (2022) 064038, http://dx.doi.org/10.1103/PhysRevD.105.064038, arXiv:2105.03079.
[25] C. Clark, W.A. Hiscock, S.L. Larson, Null geodesics in the Alcubierre warp drive space-time: The View from the bridge, Cl. Quant. Grav. 16 (1999) 3965–3972, http://dx.doi.org/10.1088/0264-9381/16/12/313, arXiv:gr-qc/9907019.
[26] P.F. Gonzalez-Diaz, On the warp drive space-time, Phys. Rev. D 62 (2000) 044005, http://dx.doi.org/10.1103/PhysRevD.62.044005, arXiv:gr-qc/9907026.
[27] A.E. Everett, Warp drive and causality, Phys. Rev. D 53 (1996) 7365–7368, http://dx.doi.org/10.1103/PhysRevD.53.7365.
[28] R.L. Arnowitt, S. Deser, C.W. Misner, The dynamics of general relativity, Gen. Relativity Gravitation 40 (2008) 1997–2027, http://dx.doi.org/10.1007/s10714-008-0661-1, arXiv:gr-qc/0405109.
[29] R.M. Wald, General Relativity, 1984.
[30] M. Alcubierre, Introduction to 3+1 Numerical Relativity, 2008.
[31] P. Painlevé, La mécanique classique et la théorie de la relativité, C. R. Acad. Sci. (Ser. Non Specifiee) 173 (1921) 677–680.
[32] A. Gullstrand, Allgemeine Lösung des statischen Einkörperproblems in der Einsteinschen Gravitationstheorie, in: Arkiv för matematik, astronomi och fysik, vol. 16,8, Almqvist & Wiksell, Stockholm, 1922.
[33] W.G. Unruh, Experimental black hole evaporation, Phys. Rev. Lett. 46 (1981) 1351–1353, http://dx.doi.org/10.1103/PhysRevLett.46.1351.
[34] M. Visser, Acoustic black holes: Horizons, ergospheres, and Hawking radiation, Cl. Quant. Grav. 15 (1998) 1767–1791, http://dx.doi.org/10.1088/0264-9381/15/6/024, arXiv:gr-qc/9712010.
[35] K. Martel, E. Poisson, Regular coordinate systems for Schwarzschild and other spherical space-times, Am. J. Phys. 69 (2001) 476–480, http://dx.doi.org/10.1119/1.1336836, arXiv:gr-qc/0001069.
[36] G.E. Volovik, The Universe in a Helium Droplet, vol. 117, 2006.
[37] C. Barcelo, S. Liberati, M. Visser, Analogue gravity, Living Rev. Rel. 8 (2005) 12, http://dx.doi.org/10.12942/lrr-2005-12, arXiv:gr-qc/0505065.
[38] V. Faraoni, G. Vachon, When Painlevé–Gullstrand coordinates fail, Eur. Phys. J. C 80 (8) (2020) 771, http://dx.doi.org/10.1140/epjc/s10052-020-8345-4, arXiv:2006.10827.
[39] G.E. Volovik, Painlevé–Gullstrand coordinates for Schwarzschild–de Sitter spacetime, Ann. Phys. 449 (2023) 169219, http://dx.doi.org/10.1016/j.aop.2023.169219, arXiv:2209.02698.
[40] W. Israel, Singular hypersurfaces and thin shells in general relativity, Nuovo Cimento B Ser. 44 (1) (1966) 1–14, http://dx.doi.org/10.1007/BF02710419.
[41] K. Lake, Thin spherical shells, Phys. Rev. D 19 (1979) 2847–2849, http://dx.doi.org/10.1103/PhysRevD.19.2847.
[42] A.H. Taub, Space-times with distribution valued curvature tensors, J. Math. Phys. 21 (1980) 1423–1431, http://dx.doi.org/10.1063/1.524568.
[43] C.K. Raju, Junction conditions in general relativity, J. Phys. A Math. Gen. 15 (6) (1982) 1785–1797, http://dx.doi.org/10.1088/0305-4470/15/6/017.

[44] C. Barrabes, W. Israel, Thin shells in general relativity and cosmology: The Lightlike limit, Phys. Rev. D 43 (1991) 1129–1142, http://dx.doi.org/10.1103/PhysRevD.43.1129.
[45] M. Mars, J.M.M. Senovilla, Geometry of general hypersurfaces in space-time: Junction conditions, Cl. Quant. Grav. 10 (1993) 1865–1897, http://dx.doi.org/10.1088/0264-9381/10/9/026, arXiv:gr-qc/0201054.
[46] R. Mansouri, M. Khorrami, Equivalence of Darmois-Israel and distributional methods for thin shells in general relativity, J. Math. Phys. 37 (1996) 5672–5683, http://dx.doi.org/10.1063/1.531740, arXiv:gr-qc/9608029.
[47] R. Steinbauer, J.A. Vickers, The Use of generalised functions and distributions in general relativity, Cl. Quant. Grav. 23 (2006) R91–R114, http://dx.doi.org/10.1088/0264-9381/23/10/R01, arXiv:gr-qc/0603078.
[48] T. Koivisto, D.F. Mota, Anisotropic Dark Energy: Dynamics of Background and Perturbations, JCAP 06 (2008) 018, http://dx.doi.org/10.1088/1475-7516/2008/06/018, arXiv:0801.3676.
[49] M. Cadoni, R. Casadio, A. Giusti, W. Mück, M. Tuveri, Effective Fluid Description of the Dark Universe, Phys. Lett. B 776 (2018) 242–248, http://dx.doi.org/10.1016/j.physletb.2017.11.058, arXiv:1707.09945.
[50] M. Cadoni, A.P. Sanna, M. Tuveri, Anisotropic fluid cosmology: An alternative to dark matter? Phys. Rev. D 102 (2) (2020) 023514, http://dx.doi.org/10.1103/PhysRevD.102.023514, arXiv:2002.06988.
[51] A. Verma, P.K. Aluri, D.F. Mota, Anisotropic universe with anisotropic dark energy, 2024, arXiv:2408.08740.
[52] L. Herrera, N.O. Santos, Local anisotropy in self-gravitating systems, Phys. Rep. 286 (1997) 53–130, http://dx.doi.org/10.1016/S0370-1573(96)00042-7.
[53] B.V. Ivanov, Static charged perfect fluid spheres in general relativity, Phys. Rev. D 65 (2002) 104001, http://dx.doi.org/10.1103/PhysRevD.65.104001, URL https://link.aps.org/doi/10.1103/PhysRevD.65.104001.
[54] W. Barreto, B. Rodriguez, L. Rosales, O. Serrano, Self-similar and charged radiating spheres: An Anisotropic approach, Gen. Relativity Gravitation 39 (2007) 23–39, http://dx.doi.org/10.1007/s10714-006-0365-3, arXiv:gr-qc/0611089; Gen.Rel.Grav. 39 (2007) 537–538, Erratum.
[55] B.V. Ivanov, Evolving spheres of shear-free anisotropic fluid, Internat. J. Modern Phys. A 25 (2010) 3975–3991, http://dx.doi.org/10.1142/S0217751X10050202, arXiv:1103.4225.
[56] V. Varela, F. Rahaman, S. Ray, K. Chakraborty, M. Kalam, Charged anisotropic matter with linear or nonlinear equation of state, Phys. Rev. D 82 (2010) 044052, http://dx.doi.org/10.1103/PhysRevD.82.044052, arXiv:1004.2165.